

Large Zero Bias Conductance Peak in Dirac Semimetal-Superconductor Devices

R. Haenel¹, W. Yu², M.A. Rodriguez², S.R. Lee², F. Zhang⁴, M. Franz¹, D. I. Pikulin⁵, and W. Pan^{2,3}

¹Stewart Blusson Quantum Matter Institute, University of British Columbia, Vancouver

³Sandia National Laboratories, Livermore, California

²Sandia National Laboratories, Albuquerque, New Mexico

⁴University of Texas at Dallas

⁵Microsoft Station Q, University of California, Santa Barbara

Summary

We report the observation of a large ZBCP in superconducting junction structures mediated by surface states of the Dirac semimetal Cd₃As₂. Our detailed analyses suggest that this large ZBCP is most likely not caused by MZMs. We attribute it, instead, to the existence of a supercurrent between two far-separated superconducting Al electrodes.

Introduction

Majorana zero modes (MZMs) are widely seen as a promising route towards the realization of topological quantum computation. One of the experimental hallmarks of the presence of MZMs is a quantized zero bias conductance peak (ZBCP) in differential conductance measurements. Here, we report the observation of such a large ZBCP in Fig. 1 in transport measurements across a Ti/Au-Cd₃As₂-Al junction.

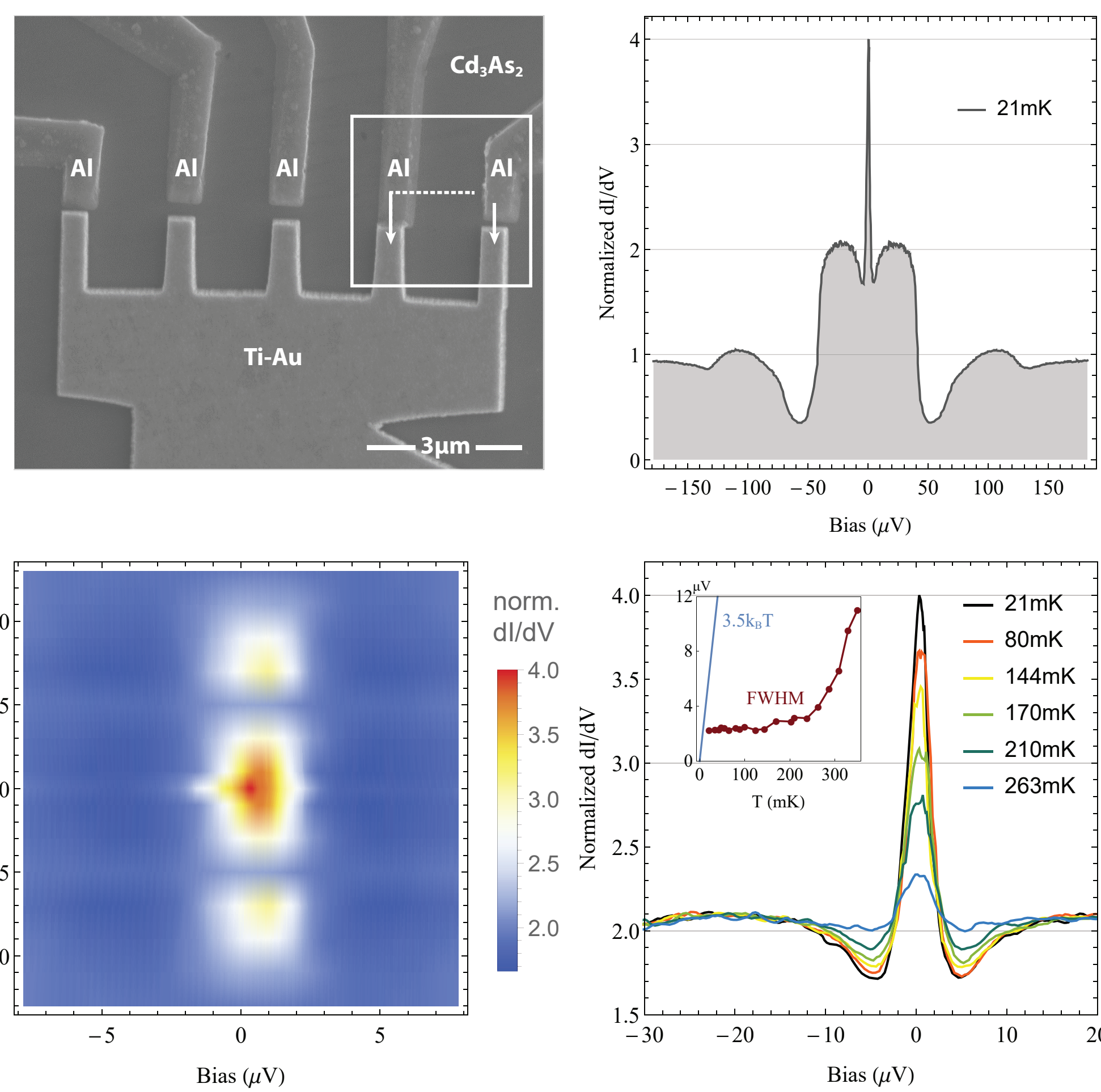


Figure 1: Device geometry and temperature and magnetic field dependence of differential conductance measured across the rightmost junction.

The upper right panel of Fig. 1 shows the differential conductance at 21 mK. The normal state conductance roughly doubles at around 50 μV as a result of perfect Andreev reflection. This indicates that a very clean interface between Cd₃As₂ and the superconducting Al electrode has been fabricated and a that gap Δ has been induced by proximity of the Al electrode. At zero bias, a sharp peak is present. The bottom panels show its magnetic field- and temperature-dependence.

Model

We model the Dirac semimetal Cd₃As₂ by the effective low energy theory

$$H_0(\mathbf{k}) = \varepsilon(\mathbf{k}) + \begin{pmatrix} M(\mathbf{k}) & Ak_- & 0 & 0 \\ Ak_+ & -M(\mathbf{k}) & 0 & 0 \\ 0 & 0 & -M(\mathbf{k}) & -Ak_- \\ 0 & 0 & -Ak_+ & M(\mathbf{k}) \end{pmatrix} \quad (1)$$

where $k_{\pm} = k_x \pm ik_y$ and $M(\mathbf{k})$, $\varepsilon(\mathbf{k})$ are even functions in \mathbf{k} [1].

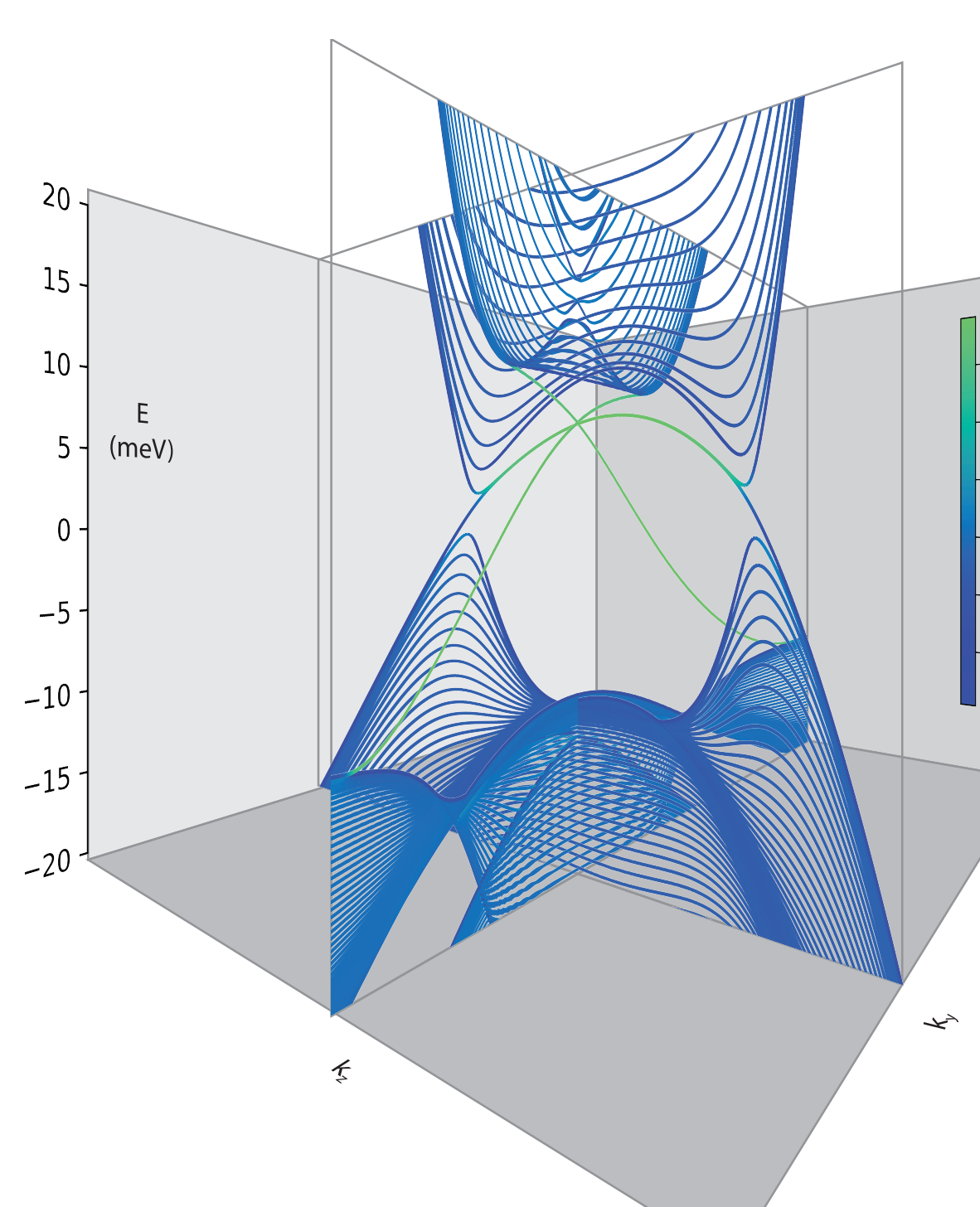


Figure 2: Bandstructure for Hamiltonian (1) with finite $L_x/a_x = 80$.

To model the junction geometry, we regularize the Hamiltonian on a lattice and add a spatially dependent superconducting order parameter Δ to obtain the BdG-Hamiltonian

$$H = \begin{pmatrix} H_0 - \mu & \Delta(x) \\ \Delta^*(x) & -(\mathcal{T}H_0\mathcal{T}^{-1} - \mu) \end{pmatrix}.$$

\mathcal{T} is the time-reversal operation with $\mathcal{T}^2 = -1$, μ is the chemical potential. In numerical simulations, we further add terms that are consistent with symmetry class DIII.

Majorana zero modes

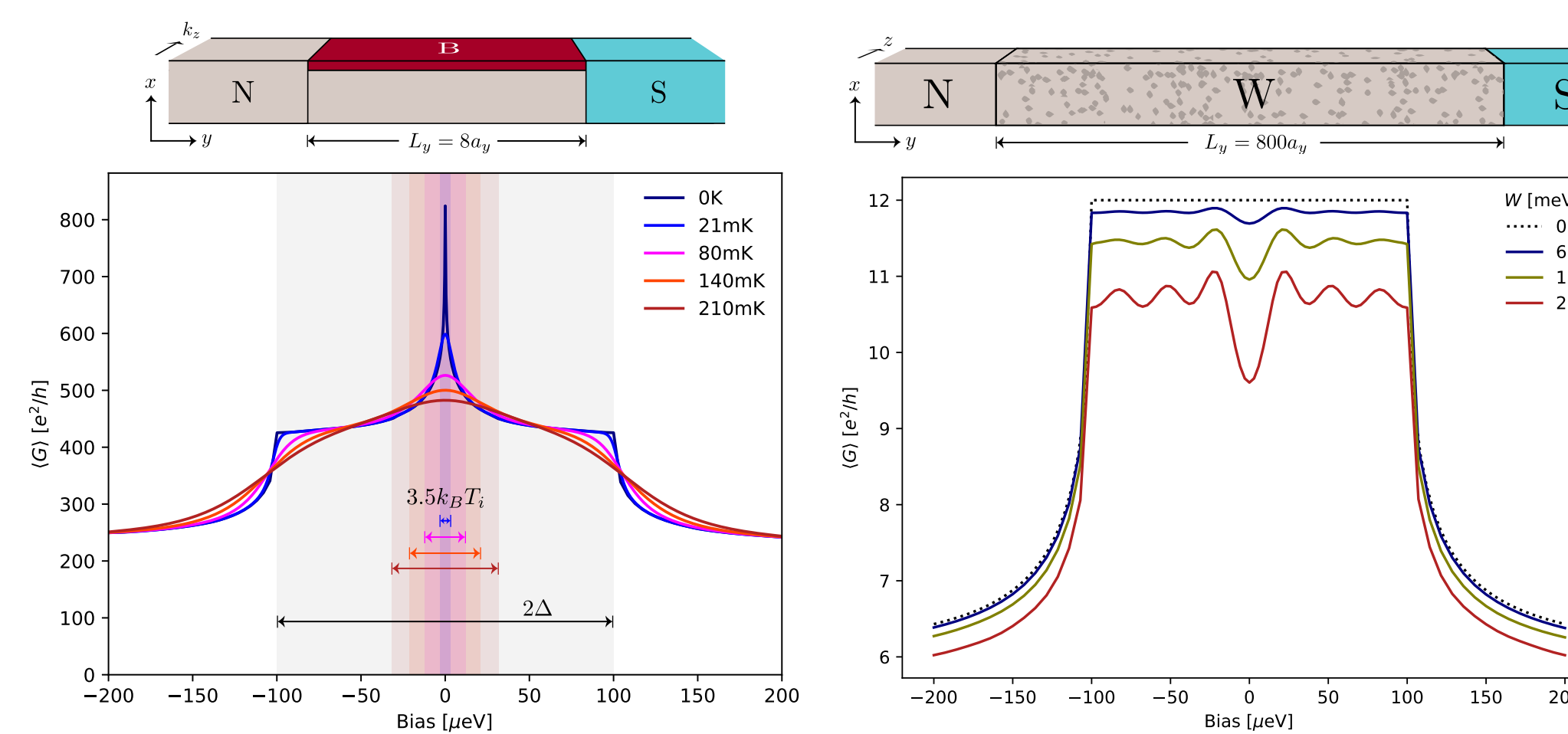


Figure 3: Transport simulations in the presence of a magnetic gap (left) and for disorder that couples QSHI for different k_z averaged over 40 realizations of disorder (right). N denotes the normal lead, S denotes the superconducting lead. The conductance dip is consistent with Weak Localization.

When k_z in Eq. (1) is treated as a parameter, the Hamiltonian describes a 2D Quantum Spin Hall insulator (QSHI). The low-energy field theory of such a QSHI is identical to the low energy description of the Kitaev chain which exhibits MZMs localized at its ends. The QSHI edge states do not have ends. However, MZMs are found at boundaries to gapped regions. Since backscattering between the edge states of a single QSHI is forbidden by \mathcal{T} , we can most easily create a gap by breaking time-reversal symmetry. A quantum transport simulation for such a scenario is shown in the left panel of Fig. 3.

A second way to create a gap and to localize MZMs involves backscattering between QSHI of different k_z . However, this approach requires fine-tuning since such scattering processes can hybridize MZMs at different k_z . We were not able to find a suitable parameter regime and instead observed a zero-bias dip consistent with Weak Localization, in disagreement to the experiment.

ZBCP due to supercurrent

Finite-temperature smearing should yield a ZBCP of width $3.5k_B T$, as exemplified in the left panel of Fig. 3. However, the experimentally observed width is much smaller (see inset of bottom right panel in Fig. 1). This strongly suggests that the ZBCP is not caused by any single-particle mechanism.

Consequently, we investigate the scenario of an additional supercurrent channel that exists between two neighboring Al-electrodes, next to the conductance channel of the NS junction. The IV relationship for a Josephson junction in the presence of thermal Nyquist noise has been derived in [2],

$$I(V) = I_0 \text{Im} \left[\frac{I_{1-2i\beta(V+R_2I)\hbar/(2e(R_1+R_2))}(\beta \frac{\hbar}{2e} I_0 \frac{\Delta(T)}{\Delta(0)})}{I_{-2i\beta(V+R_2I)\hbar/(2e(R_1+R_2))}(\beta \frac{\hbar}{2e} I_0 \frac{\Delta(T)}{\Delta(0)})} \right]. \quad (2)$$

Here, $I_n(z)$ is the modified Bessel function of the first kind. The critical current I_0 and the resistances R_1 , R_2 are treated as fit parameters.

To compare Eq. 2 to the experiment, we first subtract the linear current contribution from the NS channel, denoted by a red-dashed line in Fig. 4. The remaining contributions are in excellent agreement with the theory for a wide range of temperatures as shown in Fig. 5.

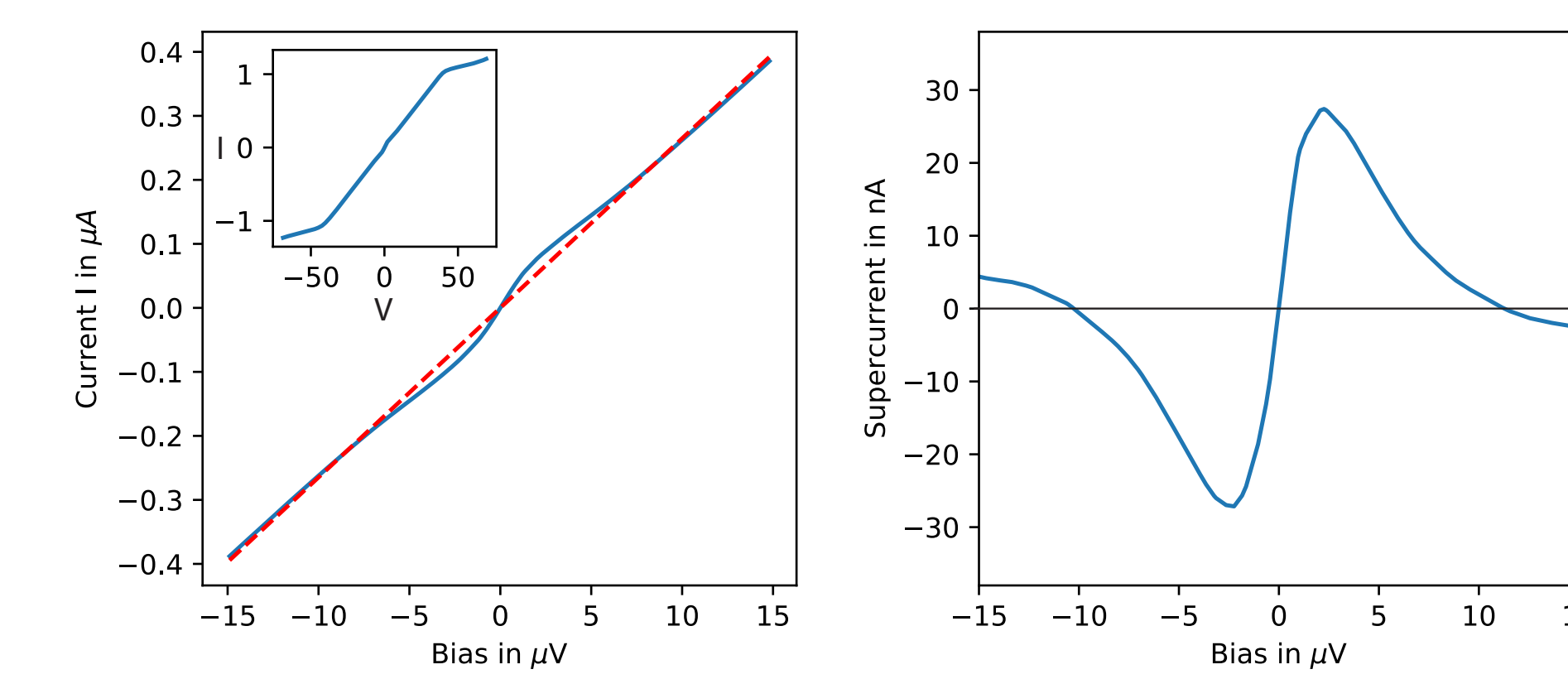


Figure 4: Experimentally measured IV-curve (left) and supercurrent contribution (right) that remains after subtracting the red-dashed linear contribution.

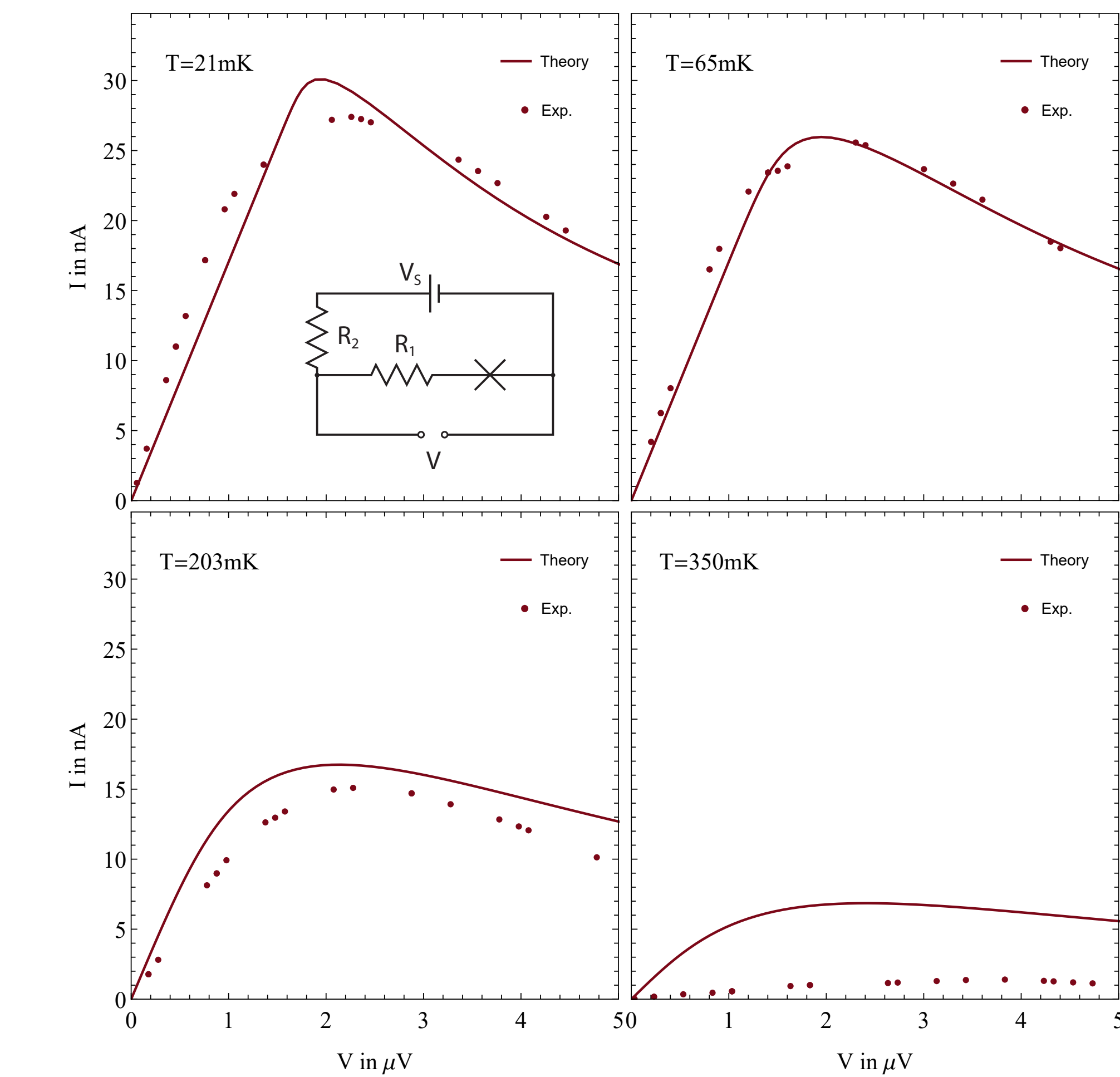


Figure 5: Experimentally measured IV curves (dots) at various temperatures agree well with the model Eq. 2 (red lines) for a wide range of temperatures. Fit parameters are $I_0 = 35$ nA, $R_1 = 59$ Ω, $R_2 = 88$ Ω. The effective circuit is depicted in the inset.

Magnetic field dependence

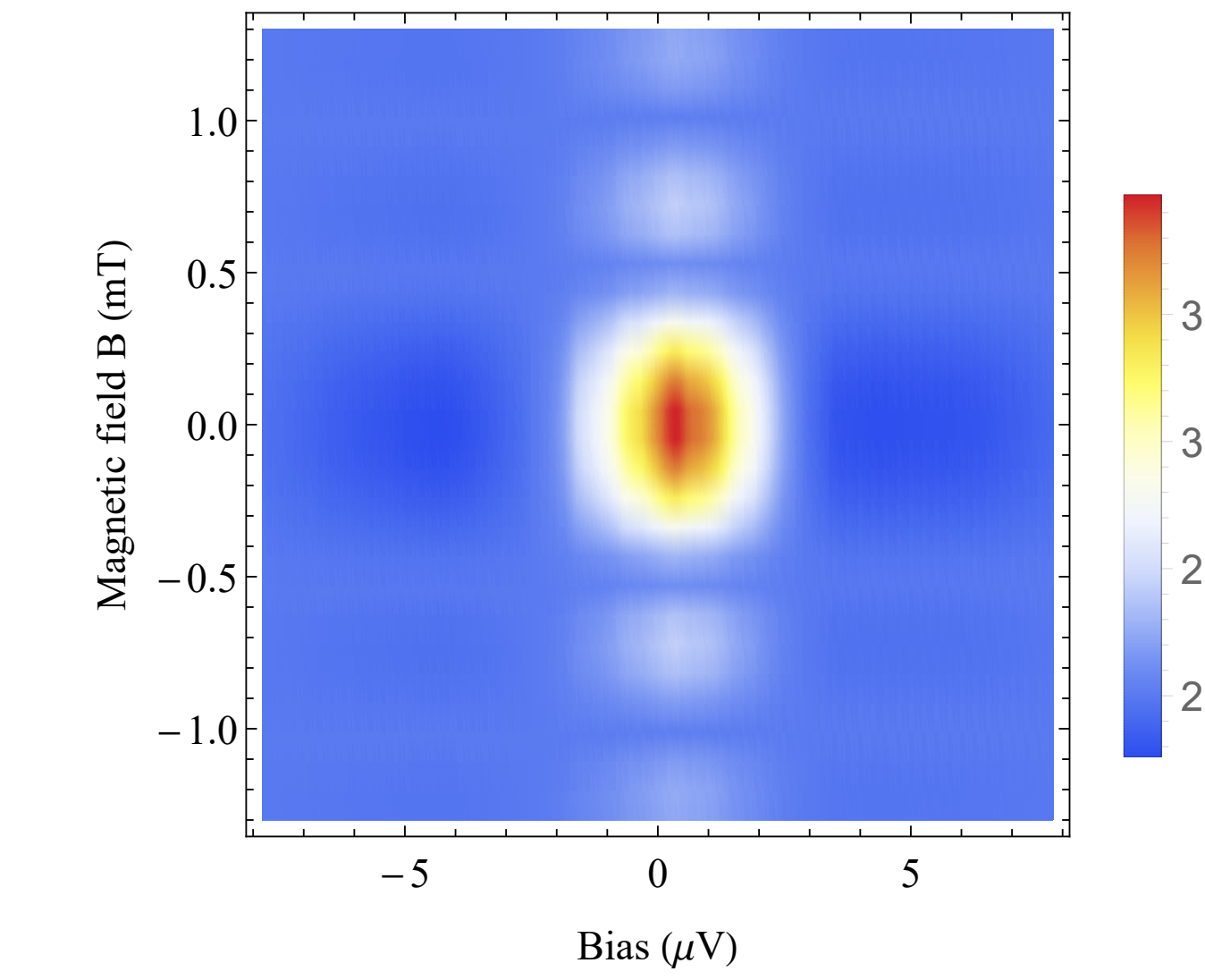


Figure 6: Simulated Fraunhofer magnetic field dependence of the differential conductance in good agreement to bottom left panel of Fig. 1.

Assuming a diffusive Josephson junction, the magnetic field dependence of the supercurrent follows the Fraunhofer interference pattern

$$I_0(\Phi) = I_0 \left| \frac{\sin(\pi\Phi/\Phi_0)}{\pi\Phi/\Phi_0} \right|.$$

Figure 6 shows the resulting simulated differential conductance assuming a junction area of $4\mu\text{m}^2$, consistent with the experimental geometry. The result is in good agreement to the experimental data.

Conclusion

In summary, we report the observation of a large ZBCP in junction structures made of normal metal (Ti/Au) – Dirac semimetal (Cd₃As₂) – conventional superconductor (Al). Our detailed analyses suggest that this large ZBCP is due to the existence of a supercurrent between two far-separated superconducting Al electrodes. Our results thus call for extreme caution when assigning a large ZBCP to the MZM origin, especially when the width of the ZBCP is below $3.5k_B T$.

References

- [1] Z. Wang, H. Weng, Q. Wu, X. Dai, and Z. Fang. Three-dimensional Dirac semimetal and quantum transport in CdAs. *Physical Review B*, 88(12):125427, 2013.
- [2] Yu M Ivanchenko and L A Zilberman. The Josephson Effect in Small Tunnel Contacts. *Soviet Physics JETP*, 28(6):1272–1276, 1969.
- [3] W. Yu, W. Pan, D.L. Medlin, M.A. Rodriguez, S.R. Lee, Zhi-qiang Bao, and F. Zhang. π and 4 π Josephson Effects Mediated by a Dirac Semimetal. *Physical Review Letters*, 120(17):177704, apr 2018.
- [4] Anffany Chen, D I Pikulin, and M Franz. Josephson current signatures of Majorana flat bands on the surface of time-reversal-invariant Weyl and Dirac semimetals. *174505:1–7*, 2017.